Rare long-range cortical connections enhance information processing

Gustavo Deco[1,2,3,4], Yonathan Sanz Perl[1], Peter Vuust[11], Enzo Tagliazucchi[5,6], Henry Kennedy[7,8] and Morten L. Kringelbach[9,10,11]

1. Center for Brain and Cognition, Computational Neuroscience Group, Department of Information and Communication Technologies, Universitat Pompeu Fabra, Roc Boronat 138, Barcelona, 08018, Spain

2. Institució Catalana de la Recerca i Estudis Avançats (ICREA), Passeig Lluís Companys 23, Barcelona, 08010, Spain

3. Department of Neuropsychology, Max Planck Institute for Human Cognitive and Brain Sciences, 04103 Leipzig, Germany

4. School of Psychological Sciences, Monash University, Melbourne, Clayton VIC 3800, Australia

5. Department of Physics, University of Buenos Aires, Argentina

6. National Scientific and Technical Research Council (CONI CET), Buenos Aires, Argentina

7. Stem Cell and Brain Research Institute, Institut National de la Santé et de la Recherche Médicale U846, 69500 Bron, France

8. Université de Lyon, Université Lyon 1, 69003 Lyon, France

9. Centre for Eudaimonia and Human Flourishing, University of Oxford, UK.

10. Department of Psychiatry, University of Oxford, Oxford, UK

11. Center for Music in the Brain, Department of Clinical Medicine, Aarhus University, DK.

Summary

A fundamental and unanswered question concerns the key topological features of connectivity that are critically relevant for generating the dynamics underlying efficient cortical function. A candidate feature that has recently emerged is that the connectivity of the mammalian cortex follows an exponential distance rule, which uniquely includes a small proportion of long-range high-weight anatomical connections. We investigate how these long-range connections influence whole-brain dynamics with coupled oscillators. To understand the causal function of long-range connections, we first studied these connections in simple ring structures and then in complex empirical brain architectures. A small proportion of long-range connections are sufficient for significantly improving information transmission, i.e. information cascade. Large-scale empirical neuroimaging modelling point to the immense functional benefits for information processing of a brain architecture with long-range coupling that improves the information cascade thanks to the underlying turbulent regime of brain dynamics.

Introduction

In Nature, complex dynamics are ubiquitous and have been shown to be fundamental in numerous model systems, ranging from the stable oscillations of the heart to turbulent fluid dynamics and brain dynamics [1-3]. Until recently, many physical systems have been successfully modelled with oscillators exhibiting short-range diffusive nearest-neighbour coupling as well as non-local exponential distance decay coupling, in this manner reflecting the nature of spatially extended physical systems. Nevertheless, the brain is a unique exception to this common coupling rule, using exceptional long-range connections that emerge from the operation of an exponential distance rule (EDR) both in non-human primates [4, 5] and rodents [6]. Here, we address the deep question concerning the role of long-range connections in the human brain and more importantly, how this unique brain architecture supports and constrains the dynamics that ensure the efficiency of information processing.

In physics, oscillators have been used to model many physical systems, going from the simplest linear, harmonic oscillator to non-linear oscillators [7]. Small perturbations to linear oscillators lead to changes in oscillation amplitudes, while perturbations to non-linear oscillators lead to self-regulating relaxation and a return to the same region in phase space. With an ordinary differential equation of a complex order parameter, the Stuart-Landau model of a single oscillator provides the simplest nonlinear extension of a linear oscillator that mathematically describes the onset of spontaneous oscillations (i.e. bifurcation from fixed-point dynamics towards a limit cycle). When dealing with a large-scale system, this obviously has to be extended to a spatially coupled system of oscillators, giving rise to a wealth of spatiotemporal patterns, ranging from regular laminar waveforms to highly turbulent dynamics.

The simplest type of spatial interaction is diffusive coupling between nearest neighbours. A continuous extension of the Stuart-Landau oscillators with diffusive coupling leads to the complex Ginzburg-Landau equation, which has been shown to accurately model many physical systems [1]. More general types of interactions can be expressed in a non-locally coupled system, assuming, for example, exponential decay in the coupling strengths as a function of distance. Kawamura, Nakao and Kuramoto demonstrated the emergence of turbulence in a supercritical regime of the system [8, 9].

Recent research using consistent tract-tracing studies shows that the anatomical architecture of the cortex reveals evidence of a similar exponential coupling of functional cortical areas [4-6]. In addition these investigations demonstrated the non-random features of the rare long-distance connections and their role in the specificity and non-homogeneity of the cortical architecture [10, 11]. Interestingly, the weight-distance relations make this architecture unique among known physical systems. However, most importantly, the functional relevance of these long-range exceptions to brain dynamics is unresolved.

Here we investigate the functional consequences of introducing long-range connections on top of the non-local coupled system of oscillators. First, we examine the functional effects of this in the simplest possible ring structures, using three different types of coupling: diffusive, exponential decay, and exponential decay with additional long-range connections. This shows that a low proportion of long-range connections critically supporting a turbulent-like regime are important to significantly improve the transmission of information across the system, i.e. the information cascade.

We investigated the effects of these topological features in the human brain. Specifically, we modelled the effects of modifying the whole-brain architecture when describing very large-scale empirical neuroimaging data from 1003 people in the human connectome project (HCP). From diffusion (dMRI) tractographic data we identified the relationship between connection weight (in tractography referred to as streamline density) and distance, and found that an EDR fits well the empirical tractographic connectivity data in the human cortex. We then identified the rare long-range exceptions, which correspond to those long-range connections with stronger weights than expected from the EDR. With whole-brain modelling we investigated the functional consequences of adding these exceptions to the EDR architecture, and again showed that this leads to a significant enhancement in fitting the empirical data and in supporting the information cascade in turbulent-like brain dynamics.

The long-range connections were in turn demonstrated to play a crucial role in the task processing underlying cognition. The results demonstrate the immense functional benefits in information processing introduced by evolution in the unique brain architecture with long-range coupling improving information cascade thanks to the underlying turbulent-like regime of brain dynamics.

Results

The study of turbulence in modern physics has led to enormous progress in the fields of fluid and oscillator dynamics [1-3]. It is well-known that coupled oscillators fit brain dynamics [12-14]. However, for the brain to function optimally, it has to support efficient information transfer and here we hypothesise that turbulence provides the intrinsic backbone necessary for brain dynamics. In particular, we hypothesise that the existence in the brain of a small proportion of long-range connections is a decisive factor for optimising information processing via the underlying turbulence. This information processing is quantitatively characterised through measures of turbulence, functional connectivity and the information cascade (**Figure 1A**).

Historically, in fluid dynamics the study of turbulence was greatly influenced by Richardson's concept of cascading eddies reflecting energy transfer (see cartoon in middle panel of **Figure 1A**), where the hierarchical organisation of different sizes of eddies is schematised for the turbulent so-

called 'inertial subrange', i.e. the range where turbulence kinetic energy is transferred without loss from large to smaller scales. Here, we propose that this hierarchical organisation of oscillators leads to an information cascade in the inertial subrange. We investigated the following quantitative measures of information processing (turbulence, functional connectivity and information cascade), first in a ring (**Figure 1B**) and then in empirical large-scale human brain data (**Figure 1C**).

Our first measure of **turbulence** comes from the study of coupled oscillators and in particular the seminal studies by Kuramoto investigating turbulence in coupled oscillators [1]. Specifically, in a coupled oscillator framework, the Kuramoto local order parameter represents a spatial average of the complex phase factor of weighted coupling of local oscillators.

Specifically, the amplitude turbulence, $R_\lambda(\bar{x},t)$, is defined as the modulus of the local order parameter for a given brain node as a function of time:

$$R_\lambda(\bar{x},t)e^{i\vartheta_\lambda(\bar{x},t)} = \mathrm{k}\int_{-\infty}^{\infty} d\bar{x}' G_\lambda(\bar{x}-\bar{x}')\, \mathrm{e}^{\mathrm{i}\varphi(\bar{x}',\mathrm{t})} \qquad (1)$$

where $\varphi(\bar{x},t)$ are the phases of the spatiotemporal data, G_λ is the local weighting kernel $G_\lambda(\bar{x}) = e^{-\lambda|\bar{x}|}$, k is the normalisation factor $[\int_{-\infty}^{\infty} d\bar{x}' G_\lambda(\bar{x}-\bar{x}')]^{-1}$ and λ is defines the scaling of local weighting. In other words, R_λ defines local levels of synchronisation at a given scale, λ, as function of space, $\bar{x}$, and time, t. This measure captures what we here call *vortex space,* R_λ, over time, inspired by the rotational vortices found in fluid dynamics, but of course not identical.

The level of amplitude turbulence is defined as the standard deviation of the modulus of Kuramoto local order parameter and can be applied to the empirical data of any physical system. The amplitude turbulence, D, corresponds to the standard deviation across time and space of R_λ:

$$D = \langle {R_\lambda}^2 \rangle_{x,t} - \langle R_\lambda \rangle_{x,t}^2 \qquad (2)$$

where the brackets $\langle \quad \rangle_{x,t}$ denotes averages across space and time.

Except for a very recent study [15], amplitude turbulence has been studied exclusively in the supercritical regime of the Stuart-Landau coupled oscillators [8, 9]. Yet, given that a range of papers have demonstrated that the Stuart-Landau oscillators fit the neuroimaging brain data when used in the subcritical regime at the edge of the bifurcation [14, 16-18], it was recently demonstrated to fit the functional MRI data from 1003 participants and to exhibit amplitude turbulence as characterised by Equation 2 [15]. The subcritical regime at the edge of the bifurcation is not showing deterministic spatiotemporal chaos in the way found in under the supercritical regime but rather some very interesting state dynamics, perhaps best described as turbulent-like or turbulent fluctuation, which are described by Equation 2. Interestingly, in the supercritical regime, turbulence is directly linked to the shear parameter of the Stuart-Landau equation, which is not needed for the subcritical regime at the brink of the bifurcation [15] and thus is not included here.

The second measure of **functional connectivity** comes from the proposal that at an abstract level information transfer is analogous to energy transfer. Indeed, the ability to facilitate fast energy transfer in fluids is one of the most relevant aspects of turbulence [3, 19, 20]. Meticulous mathematical research suggests close links between disturbance propagation and the transmission of information from one spatial point to another [2, 21]. Thus, one way to characterize information processing is to conceive functional connectivity as a function of a given distance, given by FC(r). In fact, this can be derived from Kolmogorov's concept of *structure function* for a given distance, *S(r),* of a variable *u* [19, 20] in spatiotemporal data in the following manner:

$$S(\mathrm{r}) = \langle (u(\bar{x} + r) - u(\bar{x}))^2 \rangle_{x,t} = 2[FC(0) - FC(\mathrm{r})] \qquad (3)$$

In Equation 3, the basic functional connectivity, *FC*, between two points separated by the Euclidean distance *r*, is given by:

$$FC(r) = \langle u(\bar{x} + r)u(\bar{x}) \rangle_{x,t} \qquad (4)$$

where the symbol $\langle \quad \rangle_{x,t}$ refers to the average across the spatial location $\bar{x}$ of the nodes and time. Using these relations we are able to study the impact of different architectures on the functional connectivity for long-range distances (FC long-range).

The third measure of **information cascade** uses the concept of *vortex space*, R_λ, and is defined as the average across scales, λ, of the *information cascade flow,* which indicates the predictability of a given vortex space at scale λ from the vortex space at scale $\lambda - \Delta\lambda$ (where $\Delta\lambda$ is the discretisation of scale). In other words, the measure captures information transfer across scales through local synchronization in vortex space. Mathematically, *information cascade flow* can be expressed as:

$$\mathcal{F}(\lambda) = \langle corr_t(R_\lambda(\bar{x}, t + \Delta t), R_{\lambda-\Delta\lambda}(\bar{x}, t)) \rangle_x \qquad (5)$$

where Δt is the size of the time step and where the symbol $\langle \quad \rangle_x$ refers to the spatial average of the correlation over time, $corr_t(R_\lambda, R_{\lambda-\Delta\lambda})$. The *information cascade* is the average of $\mathcal{F}(\lambda)$ across different scales, λ:

$$I = \langle \mathcal{F}(\lambda) \rangle_\lambda \qquad (6)$$

where the symbol $\langle \quad \rangle_\lambda$ refers to the average across λ.

Long-range connections in ring structure improves information processing

In order to understand the causal role of long-range connections on dynamics, we first study the simplest system, namely a ring architecture. We constructed three different types of ring architectures: nearest neighbour (NN, black ring), EDR (blue ring) and rare long-range (LR, red ring) connectivity coupling. This allowed us to create three corresponding models of coupled Stuart-

Landau oscillators, where for various scenarios we measured turbulence, averaged functional connectivity at long-range distances (FC long-range) and information cascade (**Figure 2**).

The model used a system of coupled Stuart-Landau oscillators, which is given by the following set of coupled equations:

$$\frac{dx_n}{dt} = a_n x_n - [x_n^2 + y_n^2]x_n - \omega_n y_n + G\sum_{q=1}^{N} C_{np}\left(x_q(t) - x_n\right) + \nu_n \eta_n(t) \quad (7)$$

$$\frac{dy_n}{dt} = a_n y_n - [x_n^2 + y_n^2]y_n + \omega_n x_n + G\sum_{q=1}^{N} C_{np}\left(y_q(t) - y_n\right) + \nu_n \eta_n(t) \quad (8)$$

where $\eta_n(t)$ is additive Gaussian noise with standard deviation $\nu = 0.01$. The subindex n denotes that individual oscillators are taken from (1..N=1000). Individual Stuart-Landau oscillators have a supercritical bifurcation a_n=0, so that if a_n>0, the system engages in a stable limit cycle with frequency $f_n = \omega_n/2\pi$. If a_n<0, then local dynamics are at a stable fixed point representing a low activity noisy state. Here we used the local bifurcation parameters, $a_n = -0.02$, i.e. at the brink of local bifurcations. The global coupling strength is denoted G, while C_{nq} defines the coupling matrix. In the case of the ring, we defined three different types of ring architectures with circular boundary conditions, where the nodes n are ordered sequentially.

1) Nearest neighbour (NN) ring architecture, and where $C_{nq} = 1$, if q=n±1 or $C_{nq} = 0$, otherwise.

2) The EDR ring architecture is given by

$$C_{np} = e^{-\lambda_s(r(n,p))} \quad (9)$$

Where $r(n, q)$ is the distance between nodes n and q, given by the absolute value divided by a scaling factor k=10, i.e. $|q - n|/k$. The coupling decay factor is given by $\lambda_s = 1$.

3) Rare long-range (LR) is similar to the EDR ring architecture but with additional random connections. We add these connections similar to the small-world procedure described in Watts and Strogatz [22] by going over all connections and replacing pairs randomly with a probability of p and allocating these connections a coupling strength of 0.25.

Long-range connections improve information processing in ring architecture

Figure 2 shows the three measures of turbulence, functional connectivity of long-range connections (FC long-range) and information cascade resulting from running the Stuart-Landau model in the three architectures for 1000 timesteps over 100 trials. Specifically, turbulence is computed as usual [8] at the scale $\lambda = \lambda_s$. The FC long-range was computed as the mean value of functional connectivity pairs with the top 20% largest distance. The range of scales of λ used for estimating $\mathcal{F}$ and I was given by $\lambda = [4\ 2\ 1\ 0.5\ 0.25\ 0.125\ 0.0625\ 0.0312]$.

First, **Figure 2A** shows these measures as a function of global coupling, G, in all three architectures. For the EDR+LR model, we used p=0.05 as the probability of long-range connections

and found the largest effect was on FC long-range and information cascade (compare the non-overlapping red curves with the blue and grey curves for all values of G). This means that long-range connectivity has a strong impact on information processing as revealed by the increase of functional correlations in the long-range connections and in the transmission of information reflected by the information cascade. It is interesting to note that in contrast to the other models, the NN model does not increase with G for the measures of FC long-range and information cascade. In contrast, the level of turbulence increases with G in all three architectures.

Second, **Figure 2B** shows the effect of rewiring of long-range coupling. For the optimal global coupling of the EDR+LR model, G=0.65, we plot the same three measures for all three architectures but now as a function of the probability of rewiring long-range connections. We observe the same effect as when systematically varying G and p=0.05 is close to optimal (see the red curve in the middle panel of **Figure 2B**).

Third, **Figure 2C** shows the supporting role of turbulent fluctuations on the impact of long-range connections on information processing. Here the three panels show the effect of low levels of turbulent fluctuations with a low global coupling G=0.01 in the three architectures. The boxplots reveal low levels of turbulent fluctuations for all three cases, and comparatively modest effects of long-range coupling on FC long-range and information cascade. However, **Figure 2D** shows that increases in turbulent fluctuation levels to the optimal point of the EDR+LR model, G=0.65. Under these conditions the effect of long-range connections is highly significant for both FC long-range (middle panel) and information cascade (rightmost panel).

Further insight on the low and high turbulent fluctuation regimes is provided by **Figure 2E**. Here, we investigated the EDR+LR model (with rewiring of long-range connections p=0.05) in the low (G=0.01) and high (G=0.65) turbulent fluctuation regime. The first column shows snapshots of phases associated with the low (top) and high (bottom) turbulent fluctuation regime. As can be seen, phases are more clearly clustered in the high compared to low regime, reflecting local cluster synchronisation resembling turbulent vortices. The second column shows the distribution of the FC long-range for the low (top) and high turbulent fluctuation regimes (bottom); this reveals a strong increase of the FC long-range across all pairs in the high compared to low regime.

Finally, we were able to show explicitly how information transmission across vortex space is influenced by long-range coupling. **Figure 2F** shows the *information cascade flow* (i.e. a measure *across* scales), rather than the information cascade (i.e. the *average* across scales) as shown in previous figures. As can be seen, at optimal global coupling, there is a strong effect of long-range connectivity (compare red line, p=0.05 with blue line, p=0). The baseline (grey line) is added as a reference and corresponds to the information cascade of surrogates of the same timeseries where the time-ordering of phases were shuffled (100 repeats). We show the normalised information cascade

flow (normalised with respect to baseline in the bottom plot), which shows exactly the same effect. Note in the normalised version, the flattening linear decay of information transfer for the model without long-range connections. In contrast, the EDR+LR model shows high information across all scales that decays slowly, explicitly reflecting the information cascade.

Advantage of the uniqueness of human brain architecture

The above results illustrate the advantage for information processing of adding long-range connections to a Stuart-Landau oscillator model with a simple exponential distance coupling rule on a ring. However, these results need to be corroborated with a real biological information processing system.

As stated in the introduction and shown in **Figure 3A**, the mammalian cortex is well-described by an architecture with long-range exceptions on top of an EDR [4]. The causal relevance of the two elements can be investigated with whole-brain modelling, where the key elements of EDR or EDR+LR can be manipulated and checked against the empirical data.

Given the success of fitting whole-brain models using Stuart-Landau coupled oscillators to empirical brain dynamics, we turn now our attention to demonstrate the effects of rare long-range connections in the unique brain architecture.

Reaching this goal requires a large-scale state-of-the-art dataset with both anatomical and functional dynamical data. This is available in the HCP dataset with 1003 human healthy subjects. Firstly, we find evidence that the human brain possesses a similarly unique architecture to that described in non-human primates and rodents. Secondly, we explore whole-brain modelling with Stuart-Landau oscillators so as to investigate the functional impact of different aspects -of brain architecture on information processing.

The anatomical structural connectivity of the human brain can be estimated using dMRI tractography. We estimated empirical HCP dMRI tractography of the human brain by estimating the streamline densities (i.e. connection weights) between the pairs of regions in the fine-grained Schaefer parcellations (with 1000 parcels) as a function of the Euclidian distance between nodes (**Figure 3B**). For each region pair, we computed the Euclidean distance, r, in MNI space (**Figure 3C**) in order to access the spatial information required to investigate the rules underlying coupled connectivity.

Figure 3D shows the fitting of weights of connections as a function of distance, r, by an exponential decay function. This means that the human structural anatomical connectivity exhibits a fitted EDR as reflected by the red line with an optimal $\lambda_s = 0.18$ mm^{-1} fitting the empirical mean dMRI connectivity matrix across participants (blue line). This is lower than the values $\lambda_s = 0.78$ mm^{-1} found in mice and similar to the value $\lambda_s = 0.19$ mm^{-1} found in non-human primates [4, 5].

Unlike the results in mice and non-human primates, the estimate found here is based on dMRI tractography and may be overestimating the λ_s, which is likely to be smaller. In fact, fitting the functional neuroimaging data with λ_s as a free parameter yielded values lower than the one estimated here from the structural data [15]. Nevertheless, for consistency we use the latter here. The figure also shows the remarkable similarity between the two matrices representing the empirical dMRI structural connectivity matrix (left subpanel) and the optimally fitted EDR connectivity (right subpanel).

Although dMRI is not ideal for estimating precise anatomical connections [23], we designed an algorithm to identify rare long-range outliers to the EDR, i.e. connections that are much stronger than average as derived from the EDR. This algorithm first computes the distribution of weight connections at a given distance, r, in the average dMRI connectivity matrix. We then selected only those connection pairs that are 3 standard deviations above the mean weighting of connection at that given distance, r.

We found that similar to the cortical anatomy of non-human primates and rodents [4-6], human structural anatomy is characterized by a small proportion (1.23%) of rare long-range outliers of the EDR. **Figure 3E** shows the relative percentage exceptions of long-range connections (for pairs at a given distance) as a function of that distance. Clearly, long-range outliers increase in relative percentage with increasing distances.

Furthermore, **Figure 3F** shows the relative streamline density as a function of distance for the pairs of exceptions at a given distance. Note the general trend for an increase of relative streamline density in the long-range connections, again suggesting that the EDR outliers that are expected to play a predominant role in shaping dynamics are more prevalent at longer-distances.

For visualization, **Figure 3G** shows a rendering of the combined HCP tractography in MNI space (without cerebellum and brainstem). Crucially, the edge-complete connectome can be compared with the relative simplicity of the spatial location of the long-range outliers shown in **Figure 3H**. Here, we computed the regions with long-range exceptions (larger than 40mm for the reasons outlined above) where the regions were computed as the degree of the long-range exception matrix. We render these regions on various views of the human brain. What is clear from this rendering is that the regions with long-range connections are mainly outside of primary sensory regions. Instead they are found in higher association cortex, which has been shown by many studies to be involved in higher brain function [24].

Rare long-range EDR outliers in brain architecture improve information processing

Whole-brain models offer the advantage that they can be systematically altered to fit the empirical data making it possible to test different hypotheses [25]. Here, we aimed to investigate the effect of rare long-range EDR outliers. From the empirical anatomical data, we extracted two connectivity

matrices, C_{np}, with the EDR and with long-range connections on top (EDR+LR). In this way, the human EDR matrix is implemented using Equation 9 as used for the ring architecture, but now employing three-dimensional empirical neuroimaging data. This enabled us to estimate $r(n, p)$ as the Euclidean distance between regions n and p in 3D MNI brain space, and the decay, λ_s was estimated from the human dMRI tractography as mentioned above. This yields $\lambda_s = 0.18\text{mm}^{-1}$, which is lower than the values $\lambda_s = 0.78\ \text{mm}^{-1}$ found in mice and similar to the value $\lambda_s = 0.19\ \text{mm}^{-1}$ found in non-human primates [4, 5]. And again, similar for the EDR+LR ring architecture, we estimated the long-range EDR outliers (specified above) from the human dMRI tractography and added this to the human EDR.

We used these two coupling matrices in whole-brain models of Stuart-Landau oscillators fitting the empirical functional neuroimaging from 1003 human subjects. The BOLD fMRI time series were transformed to phase space by filtering the signals in the range between 0.008-0.08 Hz and using the Hilbert transforms to extract the phase changes of the signal for each node over time (see Methods). We chose the respective optima for investigating the role of long-range connections for information processing.

The key findings are shown in **Figure 4**. In **Figure 4A**, we show the evolution of the error of the FC fitting to the empirical data for both models as a function of the global coupling strength, G. The error of the FC fitting is given by the square root of the difference between the simulated and empirical FC matrices. We found for each model an optimal working point with G_{EDR}=1.55 and G_{EDR+LR}=1.3, both with a very good level of fit to the empirical data. We used these values as the basis of the following investigations to study our two hypotheses.

Unlike the model with the ring architecture, the model with empirical brain data allows us to directly test our hypotheses. **Figure 4B** shows boxplots of the errors of the FC fitting for the two models at the corresponding optimal working point. As hypothesised, the EDR+LR with the long-range connections perform significantly better in fitting the empirical data ($p<0.001$, Wilcoxon rank sum). This confirms and extends the results from the simple ring architecture to the human brain and emphasises the important role of the long-range connections for brain function.

The model allows testing whether the long-range connections are important for real brains. Our hypothesis implies that the EDR+LR model should have increased FC long-range, whilst providing an improved fitting of the empirical data (smaller error). We focused on the absolute value of the FC long-range connections and selected pairs with long-range distances over 40 mm for the two models, repeated 100 times.

As hypothesised, the results in **Figure 4C** show a significant increase for FC long-range for the EDR+LR model ($p<0.001$, Wilcoxon rank sum). The increase in FC long-range for the EDR+LR model is concomitant with a smaller error (shown in **Figure 4B**). Thus, similar to the ring EDR+LR

model, the long-range connections in the human EDR+LR model increase the FC long-range while having a smaller fitting. The result thus confirms that this increase is what happens in real data.

Furthermore, we wanted to test our hypothesis that the long-range connections are a decisive factor for improving information processing. **Figure 4D** shows that the human EDR+LR model significantly increase information cascade ($p<0.001$, Wilcoxon rank sum) compared to the EDR model. A more detailed investigation of this is shown in **Figure 4E**, which plots the information cascade flow for the two models. Again, we found an increase for the EDR+LR model (red line) compared with EDR models (grey line) as function of the scales in vortex space. These results are in line with our hypotheses and demonstrate the functional importance of long-range connections for information processing.

We were interested in investigating other functional consequences of long-range connections in the human brain. The advantage of using a model means that we can measure the sensitivity of the model to external perturbation, which is a standard physics measure usually called susceptibility. Indeed, this measure can be obtained by perturbing the whole-brain model at the optimal working point by randomly changing the local bifurcation parameter, a_n, in the range [-0.02:0] at the node level n. Susceptibility is then estimated by measuring the modulus of the local Kuramoto order parameter, i.e. $\tilde{R}_{\lambda_s}(\bar{x},t)$ for the perturbed case, and $R_{\lambda_s}(\bar{x},t)$ for the unperturbed case. Thus, we define susceptibility s follows:

$$\chi = \langle\langle\langle\tilde{R}_{\lambda_s}(\bar{x},t)\rangle_t - \langle R_{\lambda_s}(\bar{x},t)\rangle_t)\rangle_{trials}\rangle_x \qquad (10)$$

where $\langle\ \ \rangle_t$, $\langle\ \ \rangle_{trials}$ and $\langle\ \ \rangle_x$ are the mean averages across time, trials and space, respectively. As can be seen from **Figure 4F**, again the long-range connection model outperforms the simple EDR model. Thus, the long-range connections add sensitivity to external stimulation, which could be important for task-related information processing (see below).

As a complementary measure of the effects of long-range connections on information processing, we tested the level of predictability in vortex space for q steps in the future. The predictability is computed by the correlation $corr_t(R_{\lambda_s}(\bar{x},t), R_{\lambda_s}(\bar{x},t+q))$, where $corr_t$ signifies correlation across time. As shown in **Figure 4G**, again the EDR+LR model with long-range connections outperforms the EDR model being better able to predict the future state of the brain.

Importantly, as shown in **Figure 4H**, this functional enhancement of information processing is happening in the turbulent-like regime (compare empirical, EDR+LR and EDR models). In order to show the significance of this, we constructed and computed turbulent fluctuations on surrogate data which are shuffled while maintaining the spatiotemporal characteristics of the empirical data [26]. The significant difference ($p<0.001$, Wilcoxon rank sum) offers further confirmation that turbulence provides the underlying intrinsic backbone necessary for optimal information processing. This

finding is consistent with the existence of turbulent-like empirical brain dynamics [15] but extends this by showing the explicit link to information processing.

In order to fully appreciate the spacetime evolution of turbulent fluctuations in vortex space, we have produced Supplementary movies V1 and V2, which show the spatiotemporal evolution of the local Kuramoto parameter $R_\lambda(\bar{x}, t)$ in the ring architecture and in the empirical brain data.

Finally, we were interested in providing potential evidence for the involvement of the long-range connections in the generation of resting state networks. **Figure 4I** shows the level of fitting of both models with the seven Yeo resting state networks. As can be seen both models provide good fits to the resting state networks, but the EDR+LR model is significantly better at fitting the visual, saliency, control network (CON) and default mode network (DMN) (all $p<0.001$, Wilcoxon rank sum). This important result suggests that while the EDR could well be the underlying anatomical skeleton enabling resting state networks, the long-range connections enhance the generation of the resting state networks.

Discussion

The brain appears to be unique in terms of its complex architecture spanning multiple scales. Unlike other known physical systems, where the elements communicate with nearest and close neighbouring elements (such as for example fluids or the heart), the brain uniquely possesses distant connections including a small contingent of long-range anatomical outliers, which – given their crucial role – we hypothesise have been under strong evolutionary pressure.

Here, we first use the non-invasive method of dMRI to show that the connectivity of the human cortex is similar to other animals, where large-scale tract-tracing experiments have shown that the underlying connectivity follows an EDR, where a small proportion of rare long-range outliers form connections with stronger weights than expected from the EDR. Importantly, we were able to use modelling to causally demonstrate the significant functional consequences of these rare long-range exceptions in terms of information processing.

Given that functional brain activity is well described by coupled oscillators [12, 13, 17, 18, 27], we first studied oscillators in the simplest possible ring architectures. We demonstrated that all three different ring architectures of coupled oscillators (with nearest neighbour, EDR and EDR with long-range exceptions, EDR+LR) are capable of supporting a turbulent fluctuation regime but are not all equally efficient for information transfer. Even if turbulent fluctuations are naturally suited to information transmission, we show that a small proportion of long-range connections significantly amplifies information flow as reflected in a concomitant increase of long-range FC, and, more importantly, in

the information cascade (defined as a measure of information flow providing predictability across scales).

These findings address the functional significance of the architecture principals that we examined in the human brain, where our hypothesis can be corroborated empirically. We built a whole-brain resting state model exploiting a large empirical neuroimaging dataset of 1003 human subjects. We tested our hypothesis concerning the relevance of long-range connections for information transmission by contrasting two whole-brain models, EDR and EDR+LR, structurally fitted based on the empirical anatomical connectome. In terms of function, the latter better fitted the functional empirical data and in addition showed an increase in the specific measures of long-range FC and information cascade. Importantly, the model with EDR+LR also better fitted the emergence of the classical resting-state networks. This demonstrated the potentially immense functional benefits for information processing in the turbulent fluctuation regime sustained by the brain architecture with long-range coupling.

The theoretical results from the model with the ring architecture shows that any small proportion of long-range connections can improve the information cascade (independent of their spatial location). However, the empirical results using a model with the brain architecture clearly show that these long-range exceptions are not spatially random but closely linked to the emergence of functionally important resting-state networks. Given that these networks have been shown to play a key role in task-based processing [28-30], we speculate that this suggests that evolution has improved on the basic EDR by refining long-range exceptions thereby improving brain function most notably its ability to perform certain behaviours optimising survival. This will need to be further explored in cross-species investigations.

In addition, it is of significant interest that the whole-brain model is operating in the subcritical regime at the edge of the bifurcation which means that the dynamics are not showing deterministic spatiotemporal chaos as is the case under the supercritical regime. We have decided to call the very interesting dynamics found in this regime for turbulent-like or turbulent fluctuation in order to capture the significant variability of the Kuramoto local order parameter, which is used for characterising amplitude turbulence in the supercritical regime. Indeed, this parameter describes the level of local synchronisation and therefore its variability is associated with turbulent-like fluctuations. This highly relevant turbulent-like regime for fitting empirical brain dynamics clearly warrants further investigations.

Research has investigated the hierarchical organisation of brain structure and function [31-34], which has demonstrated a common network available for the orchestration of task and rest [15]. Previous research has demonstrated that the turbulent core of brain activity is largely overlapping with brain regions known to be involved in lower level sensory processing [15]. We therefore hypothesise that the

anatomical basis of this orchestration could be well served by the long-range outliers, which effectively are able to control brain activity in the turbulent core sustained by the underlying EDR. An obvious next step would therefore be to study a task in a large empirical dataset, a challenging prospect given the difficulty at the required granularity for whole-brain models to capture the dynamical complexity specific to a given task.

Structural analysis of the cortical network has emphasised its spatial embedding, showing that weight and distance of connections are tightly interwined. Connection weights span 5 orders of magnitude and the action of the EDR means that the average connection weight declines exponentially with distance [4]. A corollary of the decline in weight is that neighbouring areas show 100% connectivity with connection densities falling to very low levels with distance. These considerations suggest that long-distance connections confer a high degree of binary specificity to the cortical network which is amply confirmed by statistical analysis [10]. Further, this analysis shows that long-distance connections carry precise signatures that ensure an important role of globalisation to a small group of areas. An intriguing finding of the present study is that the weight values of long-range connections appear to play a decisive role, given the marked differences between EDR and EDR+LR models in supporting the turbulent-like dynamics of information processing.

The present study provides a potential framework for explaining the relatively fast speed of computations needed for survival of the individual and species, which requires the fast interaction between feedforward and feedback brain connections. Given that the relatively slow average transmission delay between neurons, which is typically on the order of 40 ms between neurons, it has long been a conundrum how the brain can quickly distinguish between different categories of stimuli. Take for example the neuroimaging studies using magnetoencephalography (MEG) which have shown activity around 130-170 ms in the fusiform face area (FFA) when faces are presented (xx Kanwisher). This rapid processing is likely potentiated by scale-free network processing in the turbulent core in the sensory regions and could potentially be a purely feedforward phenomenon. Crucially, however, human neuroimaging experiments have shown that the feedback provided by the long-range exceptions must play a key role in directing the flow of information [35, 36]. As an example, MEG studies of infant and adult faces have shown activity in the FFA for both stimuli but with simultaneous activity in the orbitofrontal cortex (OFC) at around 130ms only for the infant faces [36]. Interestingly, even small deviations from the infant face template such as cleft lip, leads to much diminished activity in the OFC [37]. This ‘parental instinct’ is found in even non-parents and clearly plays a role in directing attention to the special category of infants, presumably to ensure that we provide the necessary caregiving, even when we are not the parents [38]. The long-range feedback from the OFC, presumably via the inferior longitudinal fasciculus, is controlling the rapid information processing flow, prioritising infant faces [36, 37] and sounds [39] over other less important stimuli.

The crucial functional role played by the long-range exceptions in controlling the turbulent-like core has important implications for the hierarchical organisation of brain processing. One function of the EDR is that it confers a core-periphery structure in the cortex, where the core is largely centred on the prefrontal cortex [4, 11]. The high-efficiency cortical core has been speculated to provide the structural underpinnings of the Global Workspace hypothesis [40, 41], which proposes that recurrent processing in the core allows amplification and globalization of conscious states [11, 32, 42]. These results also provide important underpinnings for other theories of consciousness such as the Integrated Information Theory (IIT) [43] and the Temporo-spatial Theory of Consciousness (TTC) [44], given that the turbulent-like regime promotes the efficient information cascade needed for spatiotemporal integration. A better and more detailed investigation of the role of particular EDR outliers is expected to give an improved understanding of the link between structure and higher cognitive function. Furthermore, since the cortical core as defined by the EDR is found across species [4-6, 45], the exploration of its involvement in turbulence across species would lead to a better understanding of comparative cognitive function.

The shaping of functional activity by a fixed anatomical structure is a conundrum that brings to mind Thomas Aquinas famous dictum: "*Quidquid recipitur ad modum recipientis recipitur*", i.e. container (or recipient) shapes the content. It has been proposed that the flexibility of brain function associated with the rich palette of behaviours is linked to changeable connectivity through for example neuromodulation [27, 46]. This *effective connectivity* is known also to change with brain states such as wakefulness, light and deep sleep. Thus, it would of considerable interest to investigate how the information cascade changes in different brain states.

In addition, we hypothesise that turbulence, information cascade and especially the lack of control of these may play a central role in neuropsychiatric disorders. The present framework would lend itself well to causally describe the emotional and information processing changes found in neuropsychiatric disorders and may provide a novel way to find sensitive and specific biomarkers.

These findings also pose a question regarding the role of long-range outliers across species. Future research could investigate the causal link between the underlying brain architecture of different species, dynamical working point, turbulence, information cascade and behavioural complexity. Ultimately, this could help cast new light on the deep question what makes us human.

Methods

Neuroimaging Ethics

The Washington University–University of Minnesota (WU-Minn HCP) Consortium obtained full informed consent from all participants, and research procedures and ethical guidelines were followed in accordance with Washington University institutional review board approval.

Neuroimaging Participants

The data set used for this investigation was selected from the March 2017 public data release from the Human Connectome Project (HCP) where we chose a sample of 1003 participants.

Schaefer parcellation

Schaefer and colleagues created a publicly available population atlas of cerebral cortical parcellation based on estimation from a large data set (N = 1489) [47]. They provide parcellations of 400, 600, 800, and 1000 areas available in surface spaces, as well as MNI152 volumetric space. We used here the Schaefer parcellation with 1000 areas and estimated the Euclidean distances from the MNI152 volumetric space and extracted the timeseries from HCP using the HCP surface space version.

Neuroimaging acquisition for fMRI HCP

The 1003 HCP participants were scanned on a 3-T connectome-Skyra scanner (Siemens). We used one resting state fMRI acquisition of approximately 15 minutes acquired on the same day, with eyes open with relaxed fixation on a projected bright cross-hair on a dark background. The HCP website (http://www.humanconnectome.org/) provides the full details of participants, the acquisition protocol and preprocessing of the data for resting state.

Preprocessing and extraction of functional timeseries in fMRI resting data

The preprocessing of the HCP resting state and task datasets is described in details on the HCP website. Briefly, the data is preprocessed using the HCP pipeline which is using standardized methods using FSL (FMRIB Software Library), FreeSurfer, and the Connectome Workbench software [48, 49]. This preprocessing included correction for spatial and gradient distortions and head motion, intensity normalization and bias field removal, registration to the T1 weighted structural image, transformation to the 2mm Montreal Neurological Institute (MNI) space, and using the FIX artefact removal procedure [49, 50]. The head motion parameters were regressed out and structured artefacts were removed by ICA+FIX processing (Independent Component Analysis followed by FMRIB's ICA-based X-noiseifier [51, 52]). Preprocessed timeseries of all grayordinates are in HCP CIFTI grayordinates standard space and available in the surface-based CIFTI file for each participants for resting state.

We used a custom-made Matlab script using the ft_read_cifti function (Fieldtrip toolbox [53]) to extract the average timeseries of all the grayordinates in each region of the Schaefer parcellation, which are defined in the HCP CIFTI grayordinates standard space. Furthermore, the BOLD time series were transformed to phase space by filtering the signals in the range between 0.008-0.08 Hz, where we chose the typical highpass cutoff to filter low-frequency signal drifts [54], and the lowpass cutoff to filter the physiological noise, which tends to dominate the higher frequencies [54, 55]. We then applied the Hilbert transforms in order to obtain the phases of the signal for each brain node as a function of the time. We computed the functional connectivity (FC) as the correlation between the BOLD timeseries in all 1000 regions in the Schaefer Parcellation.

Structural connectivity using dMRI

The Human Connectome Project (HCP) database contains diffusion spectrum and T2-weighted imaging data from 32 participants with the acquisition parameters described in details on the HCP website [56]. The freely available Lead-DBS software package (http://www.lead-dbs.org/) provides the preprocessing which is described in details in Horn and colleagues [57] but briefly, the data was processed using a generalized q-sampling imaging algorithm implemented in DSI studio (http://dsi-studio.labsolver.org). Segmentation of the T2-weighted anatomical images produced a white-matter mask and co-registering the images to the b0 image of the diffusion data using SPM12. In each HCP participant, 200,000 fibres were sampled within the white-matter mask. Fibres were transformed into MNI space using Lead-DBS [58]. We used the standardized methods in Lead-DBS to produce the structural connectomes for both Schaefer 1000 parcellation Scheme [47] where the connectivity has been normalised to a maximum of 0.2.

Stuart-Landau Model

The Stuart-Landau model consists of coupled dynamical oscillators in a given architecture. We used two different architectures: 1) ring architecture with nearest neighbour, EDR and EDR+LR coupling, and 2) anatomical brain architecture with EDR and EDR+LR coupling fitted to the empirical data. The local dynamics of each mode is described by the normal form of a supercritical Hopf bifurcation, also known as the Stuart-Landau Oscillator, which is the canonical model for studying the transition from noisy to oscillatory dynamics [59]. This has been shown to fit brain dynamics well, where the complex interactions between Hopf oscillators have been shown to reproduce significant features of brain dynamics observed in electrophysiology [12, 13], MEG [17] and fMRI [14, 18].

The dynamics of an uncoupled Stuart-Landau node n is given by the following set of coupled dynamical equations, which describes the normal form of a supercritical Hopf bifurcation in Cartesian coordinates:

$$\frac{dx_n}{dt} = a_n x_n - [x_n^2 + y_n^2]x_n - \omega_n y_n + \nu\eta_n(t) \quad (11)$$

$$\frac{dy_n}{dt} = a_n y_n - [x_n^2 + y_n^2]y_n + \omega_n x_n + \nu\eta_n(t) \quad (12)$$

where $\eta_n(t)$ is additive Gaussian noise with standard deviation ν. This normal form has a supercritical bifurcation a_n=0, so that if a_n>0, the system engages in a stable limit cycle with frequency $f_n = \omega_n/2\pi$. On the other hand, when a_n<0, the local dynamics are in a stable fixed point representing a low activity noisy state.

Acknowledgements

We would like to acknowledge the important theoretical contributions made by Profs Yoshiki Kuramoto, Hiroya Nakao, Ryan Raut and Marcus Raichle. G.D. is supported by the Spanish Research Project PSI2016-75688-P (AEI/FEDER, EU), by the European Union's Horizon 2020 Research and Innovation Programme under grant agreements n. 720270 (HBP SGA1) and n. 785907 (HBP SGA2), and by the Catalan AGAUR Programme 2017 SGR 1545. MLK is supported by the ERC Consolidator Grant: CAREGIVING (n. 615539), Center for Music in the Brain, funded by the Danish National Research Foundation (DNRF117), and Centre for Eudaimonia and Human Flourishing funded by the Pettit and Carlsberg Foundations.

References

1. Kuramoto, Y. *Chemical Oscillations,Waves, and Turbulence* (Springer-Verlag, Berlin, 1984).

2. Cross, M.C. & Hohenberg, P.C. Pattern formation outside of equilibrium. *Reviews of Modern Physics* **65**, 851-1112 (1993).

3. Frisch, U. *Turbulence: The Legacy of A. N. Kolmogorov* (Cambridge University Press, Cambridge, 1995).

4. Ercsey-Ravasz, M.*, et al.* A predictive network model of cerebral cortical connectivity based on a distance rule. *Neuron* **80**, 184-197 (2013).

5. Theodoni, P.*, et al.* Structural attributes and principles of the neocortical connectome in the marmoset monkey. *bioRxiv*, 2020.2002.2028.969824 (2020).

6. Gămănuţ, R.*, et al.* The mouse cortical connectome, characterized by an ultra-dense cortical graph, maintains specificity by distinct connectivity profiles. *Neuron* **97**, 698-715 (2018).

7. García-Morales, V. & Krischer, K. The complex Ginzburg–Landau equation: an introduction. *Contemporary Physics* **53**, 79-95 (2012).

8. Kawamura, Y., Nakao, H. & Kuramoto, Y. Noise-induced turbulence in nonlocally coupled oscillators. *Physical review. E, Statistical, nonlinear, and soft matter physics* **75**, 036209 (2007).

9. Nakao, H. Complex Ginzburg-Landau equation on networks and its non-uniform dynamics. *The European Physical Journal Special Topics* **223**, 2411-2421 (2014).

10. Markov, N.T.*, et al.* The role of long-range connections on the specificity of the macaque interareal cortical network. *Proceedings of the National Academy of Sciences of the United States of America* **110**, 5187-5192 (2013).

11. Markov, N.T.*, et al.* Cortical high-density counterstream architectures. *Science* **342**, 1238406 (2013).

12. Freyer, F.*, et al.* Biophysical mechanisms of multistability in resting-state cortical rhythms. *The Journal of neuroscience : the official journal of the Society for Neuroscience* **31**, 6353-6361 (2011).

13. Freyer, F., Roberts, J.A., Ritter, P. & Breakspear, M. A canonical model of multistability and scale-invariance in biological systems. *PLoS computational biology* **8**, e1002634 (2012).

14. Deco, G., Kringelbach, M.L., Jirsa, V. & Ritter, P. The Dynamics of Resting Fluctuations in the Brain: Metastability and its Dynamical Core [bioRxiv 065284]. *Scientific Reports* **7**, 3095 (2017).

15. Deco, G. & Kringelbach, M.L. Turbulent-like dynamics in the human brain. *Cell Reports* **33**, 108471 (2020).

16. Saenger, V.M.*, et al.* Uncovering the underlying mechanisms and whole-brain dynamics of therapeutic deep brain stimulation for Parkinson's disease [bioRxiv 083162]. *Scientific Reports* **7**, 9882 (2017).

17. Deco, G., *et al.* Single or Multi-Frequency Generators in On-going MEG Data: a Mechanistic Whole-Brain Model of empirical MEG data. *Neuroimage* **152**, 538-550 (2017).

18. Deco, G., *et al.* Awakening: predicting external stimulation forcing transitions between different brain states. *PNAS* **116**, 18088-18097 (2019).

19. Kolmogorov, A.N. The local structure of turbulence in incompressible viscous fluid for very large Reynolds numbers. *Proceedings of the USSR Academy of Sciences (in Russian)* **30**, 299-303 (1941).

20. Kolmogorov, A.N. Dissipation of Energy in Locally Isotropic Turbulence. *Proceedings of the USSR Academy of Sciences (in Russian)* **32**, 16-18 (1941).

21. Oono, Y. & Yeung, C. A cell dynamical system model of chemical turbulence. *Journal of Statistical Physics* **48**, 593-644 (1987).

22. Watts, D. & Strogatz, S. Collective dynamics of 'small-world' networks. *Nature* **393**, 440-442 (1998).

23. Donahue, C.J., *et al.* Using Diffusion Tractography to Predict Cortical Connection Strength and Distance: A Quantitative Comparison with Tracers in the Monkey. *The Journal of neuroscience : the official journal of the Society for Neuroscience* **36**, 6758-6770 (2016).

24. Buckner, R.L. & Krienen, F.M. The evolution of distributed association networks in the human brain. *Trends in cognitive sciences* **17**, 648-665 (2013).

25. Kringelbach, M.L. & Deco, G. Brain States and Transitions: Insights from Computational Neuroscience. *Cell Reports* **32**, 108128 (2020).

26. Kantz, H. & Schreiber, T. *Nonlinear time series analysis* (Cambridge University Press, Cambridge, 1997).

27. Kringelbach, M.L., *et al.* Dynamic Coupling of Whole-Brain Neuronal and Neurotransmitter Systems. *PNAS* **117**, 9566-9576 (2020).

28. Smith, S.M., *et al.* Correspondence of the brain's functional architecture during activation and rest. *Proceedings of the National Academy of Sciences of the United States of America* **106**, 13040-13045 (2009).

29. Raichle, M.E., *et al.* A default mode of brain function. *Proceedings of the National Academy of Sciences of the United States of America* **98**, 676-682 (2001).

30. Damoiseaux, J.S., *et al.* Consistent resting-state networks across healthy subjects. *Proceedings of the National Academy of Sciences of the United States of America* **103**, 13848-13853 (2006).

31. Margulies, D.S., *et al.* Situating the default-mode network along a principal gradient of macroscale cortical organization. *Proceedings of the National Academy of Sciences of the United States of America* **113**, 12574-12579 (2016).

32. Deco, G., Vidaurre, D. & Kringelbach, M.L. Revisiting the Global Workspace orchestrating the hierarchical organisation of the human brain. *Nature Human Behaviour* (2021).

33. Mesulam, M.M. From sensation to cognition. *Brain : a journal of neurology* **121**, 1013-1052 (1998).

34. Vezoli, J.*, et al.* Cortical hierarchy, dual counterstream architecture and the importance of top-down generative networks. *NeuroImage* **225**, 117479 (2020).

35. Bar, M.*, et al.* Top-down facilitation of visual recognition. *Proceedings of the National Academy of Sciences of the United States of America* **103**, 449-454 (2006).

36. Kringelbach, M.L.*, et al.* A specific and rapid neural signature for parental instinct. *PLoS ONE* **3**, e1664. doi:1610.1371/journal.pone.0001664 (2008).

37. Parsons, C.E.*, et al.* Minor structural abnormalities in the infant face disrupt neural processing: a unique window into early caregiving responses. *Soc Neurosci* **8**, 268-274 (2013).

38. Kringelbach, M.L., Stark, E.A., Alexander, C., Bornstein, M.H. & Stein, A. On cuteness: beyond caregiving to play, empathy and prosociality. *Trends Cogn Sci* **20**, 545-558 (2016).

39. Young, K.S.*, et al.* Evidence for a caregiving instinct: rapid differentiation of infant from adult vocalisations using magnetoencephalography. *Cereb Cortex* **26**, 1309-1321 (2016).

40. Baars, B.J. *A Cognitive Theory of Consciousness* (Cambridge University Press, Cambridge, MA, 1989).

41. Dehaene, S., Kerszberg, M. & Changeux, J.P. A neuronal model of a global workspace in effortful cognitive tasks. *Proceedings of the National Academy of Sciences of the United States of America* **95**, 14529-14534 (1998).

42. Mashour, G.A., Roelfsema, P., Changeux, J.-P. & Dehaene, S. Conscious processing and the global neuronal workspace hypothesis. *Neuron* **105**, 776-798 (2020).

43. Tononi, G., Sporns, O. & Edelman, G.M. A measure for brain complexity: relating functional segregation and integration in the nervous system. *Proceedings of the National Academy of Sciences of the United States of America* **91**, 5033-5037 (1994).

44. Northoff, G. What the brain's intrinsic activity can tell us about consciousness? A tri-dimensional view. *Neuroscience and biobehavioral reviews* **37**, 726-738 (2013).

45. Horvát, S.*, et al.* Spatial embedding and wiring cost constrain the functional layout of the cortical network of rodents and primates. *PLoS biology* **14**, e1002512 (2016).

46. Deco, G.*, et al.* Whole-brain multimodal neuroimaging model using serotonin receptor maps explains non-linear functional effects of LSD. *Current Biology* **28**, 3065-3074 (2018).

47. Schaefer, A.*, et al.* Local-Global Parcellation of the Human Cerebral Cortex from Intrinsic Functional Connectivity MRI. *Cerebral cortex* **28**, 3095-3114 (2018).

48. Glasser, M.F., *et al.* The minimal preprocessing pipelines for the Human Connectome Project. *NeuroImage* **80**, 105-124 (2013).

49. Smith, S.M., *et al.* Resting-state fMRI in the Human Connectome Project. *NeuroImage* **80**, 144-168 (2013).

50. Navarro Schroder, T., Haak, K.V., Zaragoza Jimenez, N.I., Beckmann, C.F. & Doeller, C.F. Functional topography of the human entorhinal cortex. *eLife* **4** (2015).

51. Salimi-Khorshidi, G., *et al.* Automatic denoising of functional MRI data: combining independent component analysis and hierarchical fusion of classifiers. *NeuroImage* **90**, 449-468 (2014).

52. Griffanti, L., *et al.* ICA-based artefact removal and accelerated fMRI acquisition for improved resting state network imaging. *NeuroImage* **95**, 232-247 (2014).

53. Oostenveld, R., Fries, P., Maris, E. & Schoffelen, J.M. FieldTrip: Open source software for advanced analysis of MEG, EEG, and invasive electrophysiological data. *Comput Intell Neurosci* **2011**, 156869 (2011).

54. Fox, M.D., *et al.* The human brain is intrinsically organized into dynamic, anticorrelated functional networks. *Proceedings of the National Academy of Sciences of the United States of America* **102**, 9673-9678 (2005).

55. Cordes, D., *et al.* Frequencies contributing to functional connectivity in the cerebral cortex in "resting-state" data. *American Journal of Neuroradiology* **22**, 1326-1333 (2001).

56. Setsompop, K., *et al.* Pushing the limits of in vivo diffusion MRI for the Human Connectome Project. *NeuroImage* **80**, 220-233 (2013).

57. Horn, A., Neumann, W.J., Degen, K., Schneider, G.H. & Kuhn, A.A. Toward an electrophysiological "sweet spot" for deep brain stimulation in the subthalamic nucleus. *Human brain mapping* **38**, 3377-3390 (2017).

58. Horn, A. & Blankenburg, F. Toward a standardized structural-functional group connectome in MNI space. *NeuroImage* **124**, 310-322 (2016).

59. Kuznetsov, Y.A. *Elements of applied bifurcation theory* (Springer, New York, 1998).

Figures

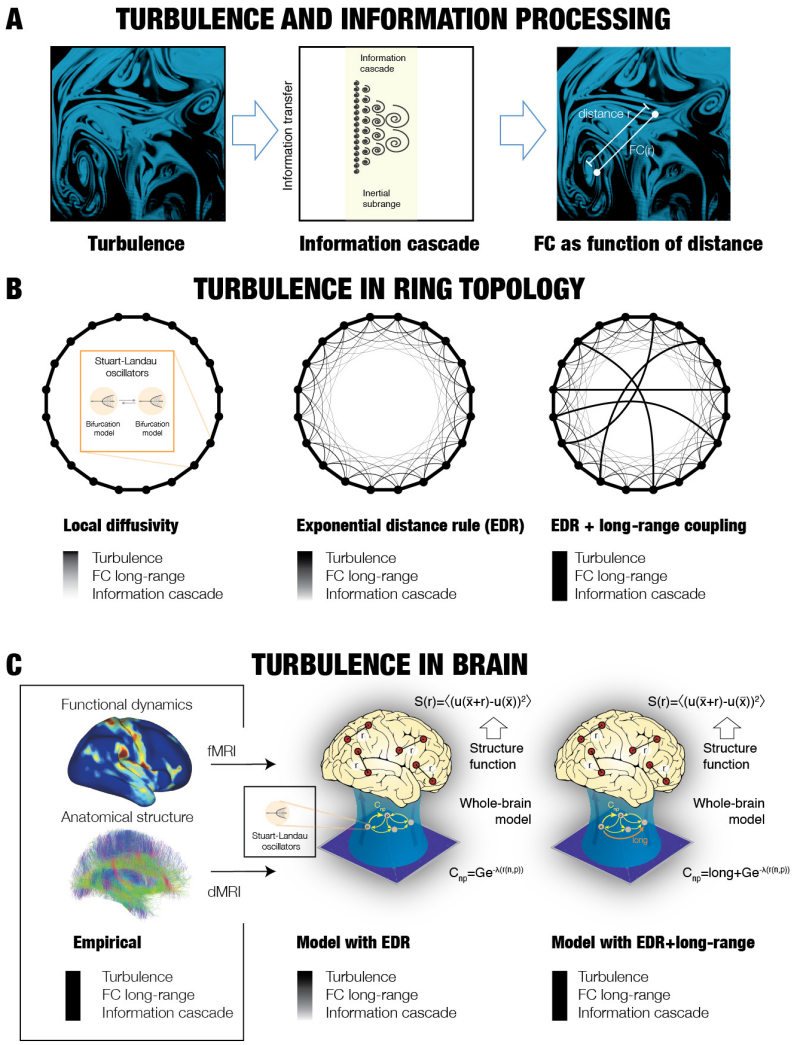

Figure 1. Overview of analysis and modelling. *We used modelling of oscillators with different architectures of coupling to study the effects on the underlying dynamics.* ***A)*** *The information processing capability of turbulence can be measured in terms of the functional connectivity (FC) as a function of distance and in terms of the efficiency of the transfer of information, i.e. the information cascade.* ***B)*** *We modelled Stuart-Landau oscillators with three distinct ring architectures of coupling: diffusive, exponential distance rule (EDR), and EDR plus a small proportion of long-range connections. For each model, we study the degree of turbulence, functional connectivity in long-range distances (FC long-range) and information cascade.* ***C)*** *We then proceed to model large-scale empirical functional neuroimaging from 1003 people in the human connectome. We fit the EDR from the anatomical dMRI connectivity data. Then we build two models with the Stuart-Landau oscillators coupled using EDR and EDR plus long-range connections. Again, we measure the resulting turbulence, FC long-range and information cascade. The best fitted results demonstrate the large impact of anatomical long-range connections on the information processing underlying brain function.*

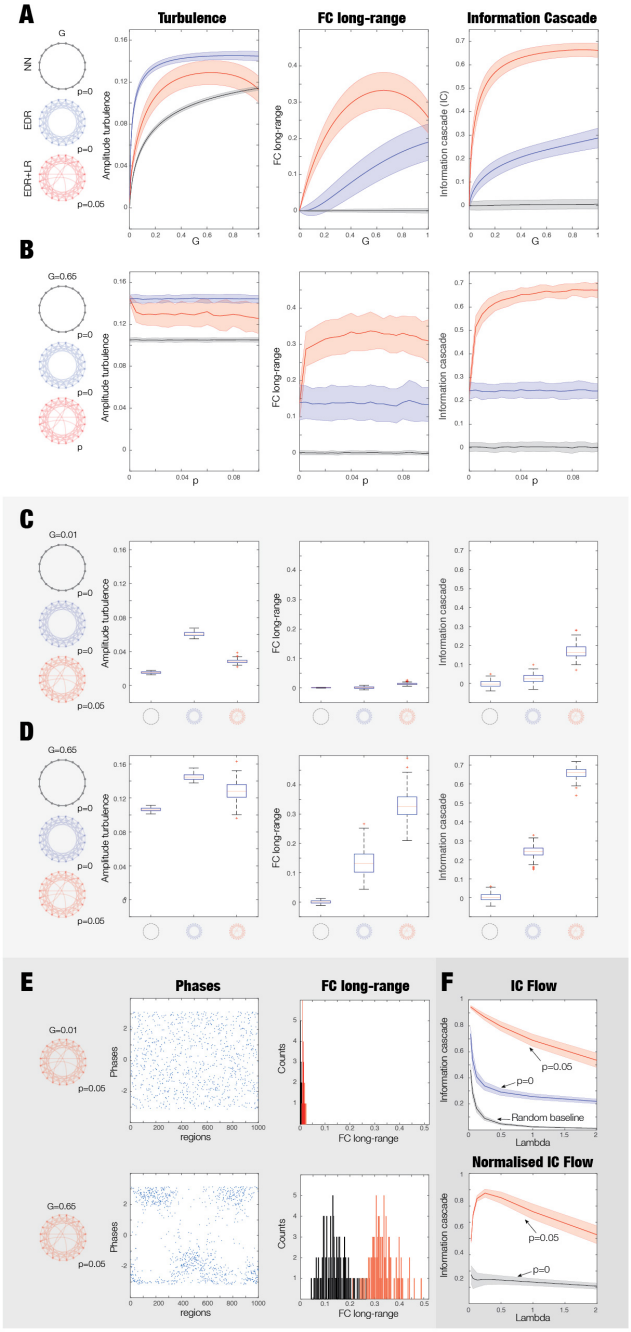

Figure 2. Long-range connections in ring structure improves information processing. *We coupled Stuart-Landau oscillators in different types of ring architectures: nearest neighbour (NN, black ring), exponential distance rule (EDR, blue ring) and EDR+long-range (LR, red ring) connections. We measured turbulence, averaged functional connectivity at long-range distances (FC long-range) and information cascade in various scenarios.* ***A)*** *First, we plot these measures as a function of global coupling, G, in the models. In the EDR+LR model, p=0.05, as the probability of long-range connections. The EDR+LR model is the best, showing long-range connectivity having a large effect on FC long-range and information cascade (compare the red curves with the blue and grey curves).* ***B)*** *Using the optimal global coupling of the EDR+LR model, G=0.65, we plot the same three*

measures but now as a function of the probability of long-range connections. Again, we find that the EDR+LR model is the best (compare the red curves with the blue and grey curves). ***C)*** *We investigated the effects of turbulence on functional connectivity and information cascade. The figure shows a row of boxplots for the measures for the three ring architectures with a low level turbulence with a low global coupling G=0.01. In this low-level of turbulence regime, the effect of the long-range connections is moderate.* ***D)*** *However, if we increase the level of turbulence at the optimal point of the EDR+LR model, G=0.65, the effect of the long-range connections is highly significant for both FC long-range (middle panel) and information cascade (rightmost panel).* ***E)*** *We were interested in comparing low and high turbulence regime and investigated the EDR+LR model with G=0.01 (low turbulence), and G=0.65 (high turbulence regime) in both cases in p=0.05. The figure shows a column with snapshots of phases in the low turbulent regime (top) and high turbulent regime (bottom). The phases are clearly more clustered for the high compared to low turbulent regime. The second column shows the distribution of the FC long-range for the low turbulent regime (top) and high turbulent regime (bottom). Again, note the strong increase of the FC long-range for the high compared to low turbulent regime.* ***F)*** *We show the information cascade flow for the three different ring architectures at the optimal global coupling, revealing the effect of the long-range connectivity. The bottom is a normalised version of the top plot with respect to the baseline (see text). This demonstrates explicitly how the information transmission across the scale of the vortex space is affected by the long-range coupling.*

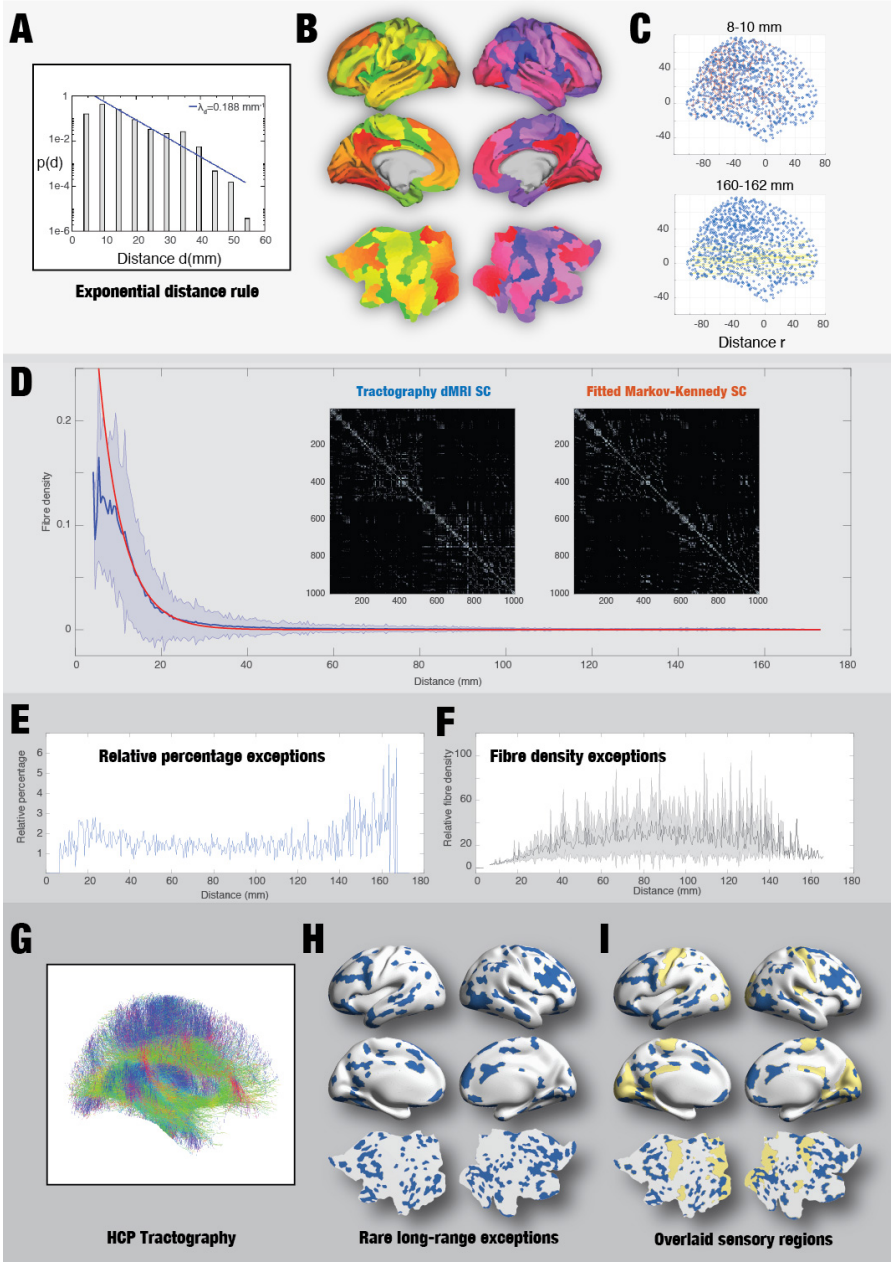

Figure 3. The human brain has a unique natural architecture with long-range anatomical connections on top of exponential distance rule (EDR). A) consistent *tract tracing studies in non-human primates have shown that most of the underlying brain connectivity follows the exponential decay described by the EDR [4]. Here is shown the histogram of interareal projection lengths for all labelled neurons (n = 6,494,974), where the blue line shows the exponential fit with a decay rate 0.19 mm^{-1}.* ***B)*** *In order to assess whether this EDR holds for the human brain, we used the fine-grained Schaefer parcellation with 1000 parcels, here shown as slices in MNI space and on the surface of the HCP CIFTI space.* ***C)*** *We computed the Euclidean distance, r, in MNI space between pairs of regions. Here we show two examples of the pairs with r=8-10 mm (top) and r=160-162 mm (bottom).* ***D)*** *We estimated the empirical HCP dMRI tractography of the human brain, as shown by the streamline densities between the pairs of regions in the Schaefer parcellations as a function of the Euclidian distance between the nodes. We found that the EDR is a good approximation of the human structural*

anatomical connectivity as shown by the red line showing the fitted EDR with an optimal $\lambda=0.18\ mm^{-1}$ fitting the empirical dMRI tractography (blue line). Equally, the remarkable similarity can be appreciated by comparing the two matrices showing the structural connectivity matrices for the empirical dMRI tractography (left subpanel) and the optimally fitted EDR connectivity (right subpanel). ***E)*** *However, our results also demonstrate that similar to the non-primates, the anatomy is also characterized by a small proportion (1.23%) of long-range outliers of the EDR. We identify an exception by computing the distribution for a given distance, and selecting those connections that are 3 standard deviations above the mean. Here, we plot the relative percentage of long-range outliers (for pairs at a given distance) as a function of that distance. Note the increase in relative percentage, especially for the longest-range connections.* ***F)*** *For these exceptions, we show relative streamline densities (for the pairs at a given distance) as a function of distance. Note the general tendency for an increase in the long-range connections.* ***G)*** *We plot a rendering of the combined HCP tractography in MNI space.* ***H)*** *The panel shows a rendering on the human brain of the regions (in blue) as a degree of the matrix of the long-range EDR outliers.* ***I)*** *Note how these EDR long-range outliers are concentrated outside of primary sensory regions (in yellow, as indexed by the myelin ratio) and instead in higher association brain regions shown by many studies to be involved in higher brain function.*

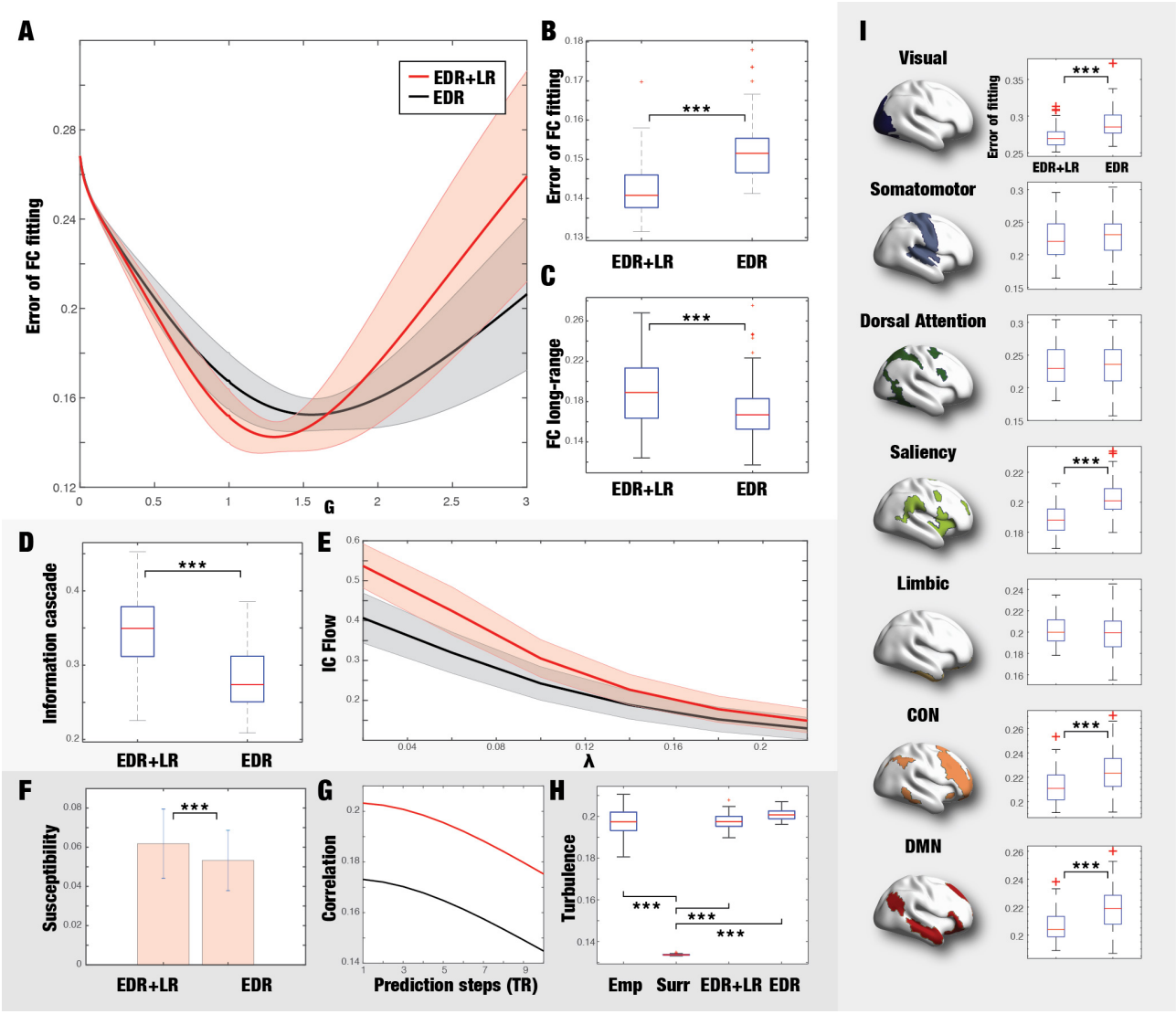

Figure 4. Whole-brain modelling shows how long-range connections in human brain improves information processing. *From the empirical anatomical data, we extracted two matrices with the exponential distance rule (EDR) and EDR+long-range (EDR+LR) connections. We then used these two coupling matrices in a whole-brain model of Stuart-Landau oscillators fitting the empirical functional neuroimaging, and chose the respective optimum for analysing the suitability of these architectures for information processing.* ***A)*** *The panel shows the error of the FC fitting to the empirical data for both models as a function of the global coupling strength, G. We use the respective minima (grey line, G_{EDR}=1.55 and red line, G_{EDR+LR}=1.3) as the basis of the following investigations.* ***B)*** *The panel shows boxplots of the errors of the FC fitting for the two models. The EDR+LR with the long-range connections perform significantly better ($p<0.001$, Wilcoxon rank sum). This extends the results from the ring architecture to the human brain and emphasises the important role of the long-range connections.* ***C)*** *The panel shows boxplots of the mean values of the FC long-range (involving pairs with distances over 40mm) for the two models across 100 trials. There is a significant increase for the EDR+LR model ($p<0.001$, Wilcoxon rank sum), which confirms the important role of long-range connections also found in the ring architecture (shown in Figure 2).* ***D)*** *Still, this raises the*

important question of the function of the long-range connections for information processing and specifically for the information cascade. The panel confirms their significant role ($p<0.001$, Wilcoxon rank sum) for increasing information cascade in the human brain architecture (compare the EDR+LR with EDR models). ***E)*** *The information cascade flow is also increased for the EDR+LR model with long-range connections (compare red line for EDR+LR and grey line for EDR models) as function of the scales in vortex space.* ***F)*** *Using whole-brain modelling allows to measure the susceptibility (the reaction to external perturbation, see text) of the two models and again the long-range connections outperform the EDR model.* ***G)*** *We can also measure the predictability in vortex space for n steps in the future (shown on x-axis). Again, the EDR+LR model with long-range connections outperforms the EDR model.* ***H)*** *Showing the amplitude turbulence for the empirical (Emp) data, surrogate (Surr) data, EDR+LR and EDR models. Both the empirical data and the two models are in the turbulent regime.* ***I)*** *The seven subpanels show brain renderings of the seven Yeo resting state networks with the corresponding boxplots of the FC fitting of the two models (smaller values are better). Again, the EDR+LR model outperforms the EDR model and is able to better fit the visual, saliency, control network (CON) and default mode network (DMN). This suggests that the long-range connections are fundamental for the generation of the classic resting state networks.*